DFT-spread OFDM with quadrature index modulation for practical VLC systems

FAHEEM AHMED, 1 D YUNGUI NIE, 1 CHEN CHEN, 1,* D MIN LIU, 1 Pengfei Du,² and Arokiaswami Alphones³

Abstract: In this paper, we for the first time propose and investigate a novel discrete Fourier transform-spread-orthogonal frequency division multiplexing with quadrature index modulation (DFT-S-OFDM-QIM) scheme for practical visible light communication (VLC) systems. By performing subcarrier index modulation on both the in-phase and quadrature components of each subcarrier, OFDM-QIM achieves a higher spectral efficiency than conventional OFDM with index modulation (OFDM-IM). Moreover, the peak-to-average power ratio (PAPR) of OFDM-QIM can be substantially reduced by applying DFT spreading, and hence DFT-S-OFDM-QIM exhibits high tolerance against light-emitting diode (LED) nonlinearity. The superiority of the proposed DFT-S-OFDM-QIM scheme over other benchmark schemes has been successfully verified by both simulation and experimental results.

© 2021 Optical Society of America under the terms of the OSA Open Access Publishing Agreement

Introduction

In recent years, visible light communication (VLC) has been envisioned as one of the key enabling technologies for 6G and Internet of Things (IoT) systems [1–3]. By leveraging commercial offthe-shelf (COTS) light emitting diodes (LEDs) for simultaneous illumination and communication, VLC enjoys many inherent advantages such as abundant and license-free spectrum resources, low-cost front-ends, no electromagnetic interference (EMI) radiation and enhanced physical-layer security [4]. However, practical VLC systems built upon COTS LEDs face two critical challenges: one is the limited available modulation bandwidth and the other is the severe nonlinearity [5,6].

So far, many techniques have been introduced to address the two challenges faced by practical VLC systems. On the one hand, in order to break the bandwidth limitation of COTS LEDs, their available modulation bandwidth can be efficiently extended by applying various analog or digital equalization techniques [7–9]. Moreover, for a given modulation bandwidth, the available data rate of VLC systems can also be improved by applying spectral-efficient modulation techniques. Specifically, orthogonal frequency division multiplexing (OFDM) with high-order quadrature amplitude modulation (QAM) constellations has been widely considered in high-speed VLC systems [10–12]. In addition, spectral-efficient multiple access techniques such as non-orthogonal multiple access (NOMA) can also be adopted to enhance the achievable data rate for a given modulation bandwidth [13–16]. On the other hand, in order to address the LED nonlinearity issue, distortion techniques have been proposed to linearize the overall system nonlinearity [17], while nonlinear equalizers have been designed to mitigate the adverse effect of LED nonlinearity [18,19]. Furthermore, for a given nonlinear characteristic of LED, its adverse effect can be mitigated by transmitting signals with low peak-to-average power ratio (PAPR). Hence, spectral-efficient OFDM modulation with reduced PAPR can be a promising candidate for practical VLC systems [17].

 $^{^{}I}$ School of Microelectronics and Communication Engineering, Chongaing University, Chongaing 400044,

²A*STAR's Singapore Institute of Manufacturing Technology (SIMTech), 138634, Singapore

³School of Electrical and Electronic Engineering, Nanyang Technological University, 639798, Singapore *c.chen@cqu.edu.cn

Lately, OFDM with index modulation (OFDM-IM) has been proposed as a novel multi-carrier transmission scheme for 5G wireless networks, which has been shown to be able to achieve better bit error rate (BER) performance than classical OFDM [20]. In OFDM-IM, the information bits are conveyed not only by the M-ary signal constellations, but also by the indexes of the subcarriers [21]. Due to its excellent BER performance, OFDM-IM has already been applied in VLC systems [22,23]. Nevertheless, it is challenging for OFDM-IM-based VLC systems to obtain high spectral efficiency (SE). As an enhanced version of OFDM-IM, OFDM with quadrature index modulation (OFDM-QIM) has been further proposed for SE improvement, where subcarrier index modulation is performed on both the in-phase and quadrature components of each subcarrier [24]. Nevertheless, since only a subset of subcarriers are activated to transmit constellation information in both OFDM-IM and OFDM-QIM, the spectral efficiencies of OFDM-IM and OFDM-QIM might be lower than that of classical OFDM. Hence, OFDM-IM and OFDM-QIM are generally suitable for low-SE applications where a relatively small constellation size is required, e.g., cell edge of a practical cellular VLC system [25]. Moreover, OFDM-IM and OFDM-QIM can achieve a finer-grained spectral efficiency than classical OFDM. However, both OFDM-IM and OFDM-QIM suffer from high PAPR as classical OFDM, which might not be suitable for practical VLC systems with LED nonlinearity.

In this paper, we for the first time propose a novel discrete Fourier transform (DFT)-spread OFDM-QIM (DFT-S-OFDM-QIM) scheme for practical VLC systems relying on COTS LEDs. By performing DFT spreading, the PAPR of OFDM-QIM can be substantially reduced and hence DFT-S-OFDM-QIM exhibits high tolerance against LED nonlinearity. Both simulations and experiments have been conducted to verify the superiority of the proposed DFT-S-OFDM-QIM scheme over other benchmark schemes.

2. Principle of DFT-S-OFDM-QIM

Figures 1(a) and (b) illustrate the block diagrams of the DFT-S-OFDM-QIM transmitter and receiver, respectively. In the DFT-S-OFDM-QIM transmitter, a total of b information bits enter the bit splitter, which are divided into G groups and every group has p bits, i.e., b = pG. Every p bits is used to generate the in-phase and quadrature components of an OFDM subblock of length N, where $N = N_{\rm data}/G$ and $N_{\rm data}$ is the number of data subcarriers within each OFDM block. More specifically, the input p bits of each OFDM subblock mainly consist of three parts: 1) $p_{\rm C}$ bits are first sent into the M-QAM mapper to generate the complex-valued M-QAM constellation symbols, whose in-phase and quadrature parts are then separated via an I/Q separator; 2) $p_{\rm I}$ bits are fed into the in-phase index selector to identify the indexes of k out of N subcarriers which are activated to transmit the in-phase parts of the M-QAM constellation symbols; 3) $p_{\rm Q}$ bits are fed into the quadrature index selector to select the indexes of k out of N subcarriers which are activated to transmit the quadrature parts of the M-QAM constellation symbols. Hence, we have $p = p_{\rm C} + p_{\rm I} + p_{\rm Q}$. In the g-th ($g = 1, 2, \ldots, G$) OFDM subblock, the set of indexes of the selected subcarriers corresponding to both the in-phase and quadrature parts is denoted by $I_g = \left\{I_g^{\rm I}, I_g^{\rm Q}\right\}$, and we have

$$I_g^{\rm I} = \left\{ i_{g,1}^{\rm I}, \dots, i_{g,k}^{\rm I} \right\}, \ I_g^{\rm Q} = \left\{ i_{g,1}^{\rm Q}, \dots, i_{g,k}^{\rm Q} \right\},$$
 (1)

where $i_{g,\gamma}^{I}$, $i_{g,\gamma}^{Q} \in \{1,\ldots,N\}$ for $\gamma = 1,\ldots,k$. Therefore, the in-phase and quadrature signals in the *g*-th OFDM subblock are obtained by

$$x_{g,\eta}^{\mathrm{I}} = \begin{cases} s_{g,\eta}^{\mathrm{I}}, & \eta \in I_{g}^{\mathrm{I}} \\ 0, & \text{otherwise} \end{cases}, x_{g,\eta}^{\mathrm{Q}} = \begin{cases} s_{g,\eta}^{\mathrm{Q}}, & \eta \in I_{g}^{\mathrm{Q}} \\ 0, & \text{otherwise} \end{cases},$$
 (2)

where $s_{g,\eta}^{\rm I}$ and $s_{g,\eta}^{\rm Q}$ for $g=1,\ldots,G$ and $\eta=1,\ldots,N$ denote the corresponding in-phase and quadrature parts of the M-QAM constellation symbols, respectively. After that, the obtained

in-phase and quadrature signals are combined to yield the output of the g-th OFDM subblock as follows:

$$x_{g,\eta} = x_{g,\eta}^{I} + jx_{g,\eta}^{Q}. (3)$$

Subsequently, a complete OFDM block is created by concatenating totally *G* OFDM subblocks. In order to reduce the PAPR of the OFDM-QIM signal, DFT spreading is further performed. After executing inverse fast Fourier transform (IFFT) with the Hermitian symmetry (HS) constraint and parallel-to-serial (P/S) conversion, the transmitted DFT-S-OFDM-QIM signal is finally obtained.

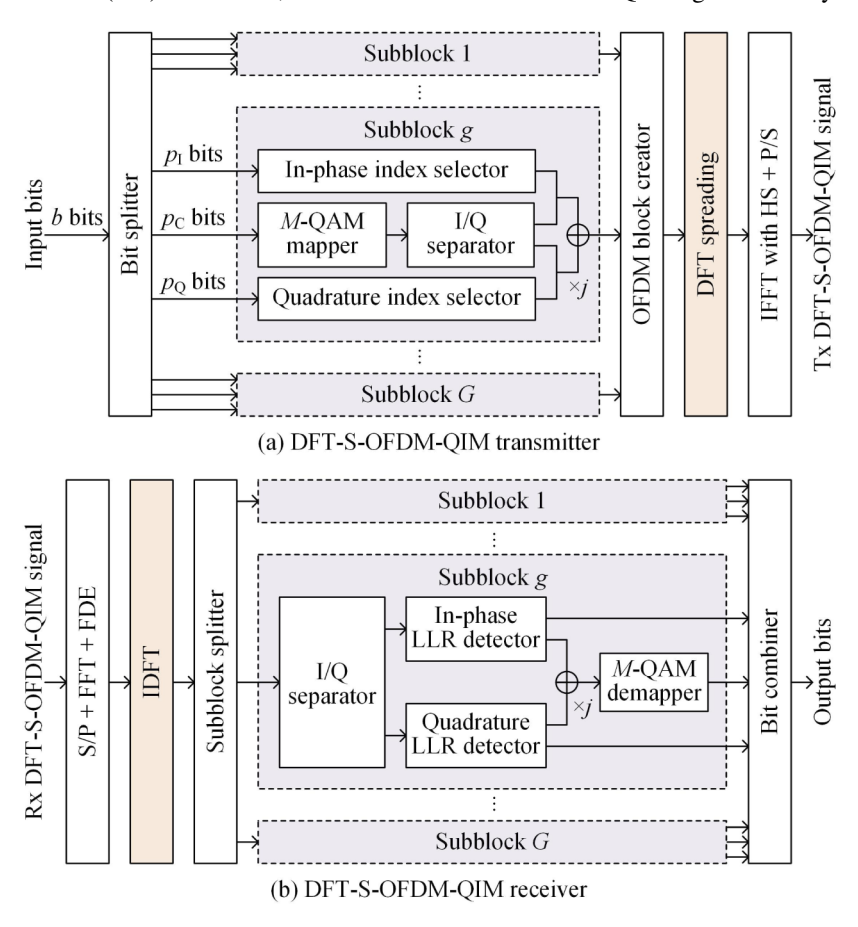


Fig. 1. Block diagrams of DFT-S-OFDM-QIM (a) transmitter and (b) receiver.

In the DFT-S-OFDM-QIM receiver, as shown in Fig. 1(b), the received serial DFT-S-OFDM-QIM signal is first converted into a parallel signal through serial-to-parallel (S/P) conversion. After performing FFT and frequency-domain equalization (FDE), inverse DFT (IDFT) is executed before the OFDM block is divided into G subblocks via subblock splitter. In each subblock, the in-phase and quadrature components of the input complex-valued signal are first extracted via an I/Q separator. Then, log-likelihood ratio (LLR) detection is carried out individually with respect to both the in-phase and quadrature components of the input complex-valued signal [24]. Letting $y_{g,\eta}$ ($g=1,2,\ldots,G; \eta=1,\ldots,N$) be the input complex-valued signal, the corresponding LLR values for the g-th OFDM subblock are calculated by

$$\lambda_{g,\eta}^{I} = \ln(k) - \ln(N - k) + \frac{\left| \text{Re}(y_{g,\eta}) \right|^{2}}{N_{0}} + \ln \left(\sum_{m=1}^{M^{I}} \exp\left(-\frac{1}{N_{0}} \left| \text{Re}(y_{g,\eta}) - s_{m}^{I} \right|^{2} \right) \right), \tag{4}$$

$$\lambda_{g,\eta}^{Q} = \ln(k) - \ln(N - k) + \frac{\left| \text{Im}(y_{g,\eta}) \right|^{2}}{N_{0}} + \ln\left(\sum_{m=1}^{M^{Q}} \exp\left(-\frac{1}{N_{0}} \left| \text{Im}(y_{g,\eta}) - s_{m}^{Q} \right|^{2} \right) \right), \tag{5}$$

where $\text{Re}(\cdot)$ and $\text{Im}(\cdot)$ denote the operations to extract the in-phase and quadrature parts of a complex-valued input, respectively; N_0 denotes the noise power; s_m^I and s_m^Q respectively represent the one-dimensional constellations corresponding to the in-phase and quadrature components of the two-dimensional M-QAM constellation, and M^I and M^Q are the corresponding numbers of the one-dimensional constellation points. It should be noted that $M^I = M^Q = \sqrt{M}$ when square M-QAM constellations are adopted in the DFT-S-OFDM-QIM system. Moreover, due to the parallel index modulation in both in-phase and quadrature components, the detection complexity of DFT-S-OFDM-QIM is twice as that of DFT-S-OFDM-IM. After LLR detection in each subblock, the corresponding M-QAM constellation symbols are recovered which are further demapped to recover the constellation bits. Finally, the output bits can be generated by combining the obtained in-phase index bits, quadrature index bits and the constellation bits together via a bit combiner.

For VLC systems using DFT-S-OFDM-QIM with M-QAM constellation, the number of bits that can be transmitted in one OFDM subblock with length N and k activated subcarriers is obtained by

$$b_{\text{DFT-S-OFDM-OIM}} = p_{\text{I}} + p_{\text{O}} + p_{\text{C}} = 2|\log_2(C(N,k))| + k\log_2(M),$$
 (6)

where $\lfloor \cdot \rfloor$ represents the floor operator and $C(\cdot, \cdot)$ denotes binomial coefficient. Therefore, the SE per OFDM block using DFT-S-OFDM-QIM with M-QAM constellation is expressed by

$$SE_{\text{DFT-S-OFDM-QIM}} = \frac{b_{\text{DFT-S-OFDM-QIM}}}{N} = \frac{2\lfloor \log_2(C(N,k)) \rfloor + k \log_2(M)}{N}.$$
 (7)

Moreover, for the purpose of comparison, the SE per OFDM block using DFT-S-OFDM-IM with *M*-QAM constellation is also given as follows:

$$SE_{\text{DFT-S-OFDM-IM}} = \frac{\lfloor \log_2(C(N,k)) \rfloor + k \log_2(M)}{N}.$$
 (8)

It can be clearly observed from (7) and (8) that the proposed DFT-S-OFDM-QIM scheme can transmit a doubled number of index bits in comparison to DFT-S-OFDM-IM.

3. Results and discussions

In this section, we evaluate the performance of the proposed DFT-S-OFDM-QIM scheme and compare it with other three benchmark schemes including OFDM-IM, DFT-S-OFDM-IM and OFDM-QIM through both numerical simulations and hardware experiments. In both simulations and experiments, the size of IFFT/FFT is set to 256, the length of each OFDM subblock is N=4 and the number of activated subcarriers in each subblock is k=1, 2. Moreover, the numbers of data subcarriers are set to $N_{\rm data}=118$ and 108 for k=1 and 2, respectively. In addition, we adopt 4-QAM constellation for the proposed DFT-S-OFDM-QIM, and hence the corresponding SEs for k=1 and 2 are 1.5 and 2 bits/s/Hz, respectively. The required M-QAM constellations to achieve a target SE for four schemes are summarized in Table 1.

3.1. Simulation results

In this subsection, we evaluate and compare the performance of OFDM-IM, DFT-S-OFDM-IM, OFDM-QIM and DFT-S-OFDM-QIM via numerical simulations. Figures 2(a) and (b) show the BER versus signal-to-noise ratio (SNR) for four schemes over the additive white Gaussian noise (AWGN) channel with N = 4, k = 1 and N = 4, k = 2, respectively. For the case of N = 4

Schemes.		
Scheme	SE = 1.5 bits/s/Hz (N = 4, k = 1)	SE = 2 bits/s/Hz (N = 4, k = 2)
OFDM-IM	16-QAM	8-QAM
DFT-S-OFDM-IM	16-QAM	8-QAM
OFDM-QIM	4-QAM	4-QAM
DFT-S-OFDM-QIM	4-QAM	4-QAM

Table 1. Required M-QAM constellations to achieve a target SE for four schemes.

and k=1, as shown in Fig. 2(a), the required SNRs for OFDM-IM and OFDM-QIM to reach the 7% forward error correction (FEC) coding limit of BER = 3.8×10^{-3} are 9.4 and 6.3 dB, respectively, indicating that OFDM-QIM outperforms OFDM-IM by an SNR gain of 3.1 dB. However, as shown in Fig. 2(b), the SNR gain of OFDM-QIM in comparison to OFDM-IM is reduced to only 1.6 dB for N=4 and k=2. The reduction of SNR gain when k is increased from 1 to 2 is mainly due to the decrease of constellation order required by OFDM-IM as given in Table 1. Moreover, it can also be clearly observed that, for both OFDM-IM and OFDM-QIM, performing DFT spreading does not affect their BER performance.

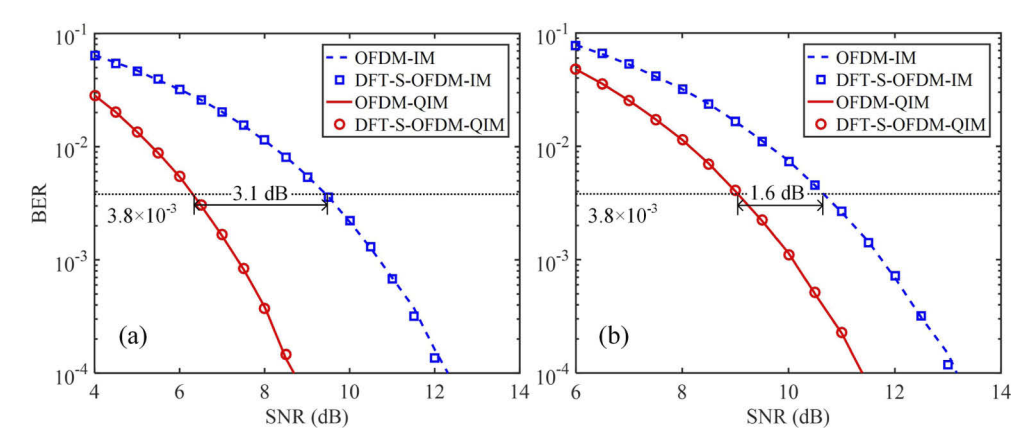


Fig. 2. BER vs. SNR for OFDM-IM, DFT-S-OFDM-IM, OFDM-QIM and DFT-S-OFDM-QIM over the AWGN channel with (a) N = 4, k = 1 and (b) N = 4, k = 2.

Although maximum-likelihood (ML) detection is the optimal detection scheme for DFT-S-OFDM-QIM, it has high computational complexity. Instead, LLR detection is a low-complexity scheme which is adopted in our work here. Figure 3 compares the performance of LLR detection and ML detection for DFT-S-OFDM-QIM over the AWGN channel with N=4 and k=1,2. It can be clearly seen that the low-complexity LLR detection achieves nearly the same BER performance as the optimal ML detection for both N=4, k=1 and N=4, k=2.

Figure 4 further compares the PAPR performance of OFDM-IM, DFT-S-OFDM-IM, OFDM-QIM and DFT-S-OFDM-QIM. For the case of N=4 and k=1, as shown in Fig. 4(a), the use of DFT spreading cannot reduce the PAPR of OFDM-IM. Instead, OFDM-IM performs about 1-dB better than DFT-S-OFDM-IM at a probability of 10^{-3} . In contrast, the PAPR of OFDM-QIM can be efficiently reduced by 1.6 dB at a probability of 10^{-3} by applying DFT spreading. Moreover, for the case of N=4 and k=2, DFT-S-OFDM-IM only slightly outperforms OFDM-IM, while DFT-S-OFDM-QIM significantly outperforms OFDM-QIM. It can be seen from Fig. 4(b) that a PAPR reduction of 2.8 dB is obtained by DFT-S-OFDM-QIM compared with OFDM-QIM. As a result, DFT spreading is shown to be an efficient approach to substantially reduce the PAPR of OFDM-QIM for both cases.

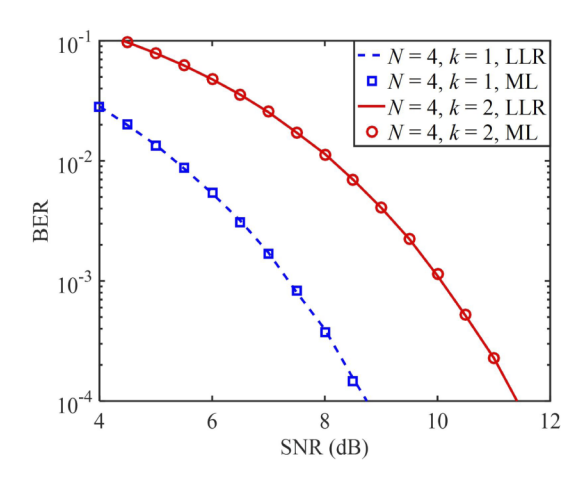


Fig. 3. Comparison of LLR detection and ML detection for DFT-S-OFDM-QIM over the AWGN channel with N=4 and k=1,2.

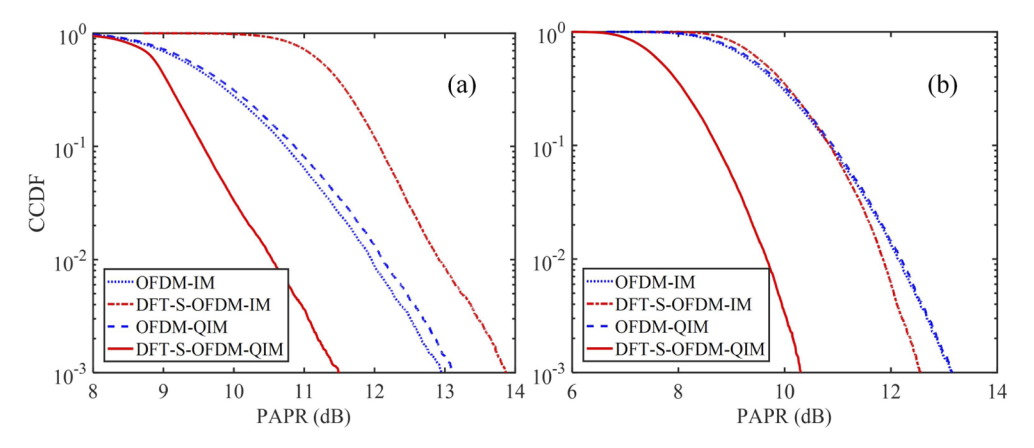


Fig. 4. PAPR comparison of OFDM-IM, DFT-S-OFDM-IM, OFDM-QIM and DFT-S-OFDM-QIM with (a) N=4, k=1 and (b) N=4, k=2.

3.2. Experimental results

In this subsection, we conduct experiments to investigate the performance of DFT-S-OFDM-QIM in a practical nonlinear VLC system and further compare it with other benchmark schemes. Figure 5 illustrates the experimental setup of a point-to-point VLC system using a blue mini-LED. The transmitted signal is first digitally generated offline by MATLAB, which is then loaded into an arbitrary waveform generator (AWG, Tektronix AFG31102) with a sampling rate of 250 MSa/s. A 120-mA DC bias current is further added to the AWG output via a bias-tee (Mini-Circuits, ZFBT-6GW+) and the combined signal is subsequently used to drive a blue mini-LED (HCCLS2021CHI03). At the receiver side, the optical signal is detected by a photodetector (PD, Thorlabs PDA10A2) with a bandwidth of 150 MHz and an active area of 0.8 mm². The received electrical signal is recorded by a digital storage oscilloscope (DSO, LeCroy WaveSurfer 432) with a sampling rate of 1 GSa/s and further demodulated offline in MATLAB. Moreover, a pair of biconvex lenses each with a diameter of 12.7 mm and a focal length of 20 mm are also employed to align the LED and the PD. The inset (a) in Fig. 5 shows the photo of the overall experimental system. The measured nonlinear optical power-current curve and the low-pass frequency response of the system are given by the insets (b) and (c), respectively. As we can

see, the experimental system exhibits notable nonlinearity which is mainly caused by the blue mini-LED. Moreover, a larger bandwidth can be obtained when a larger bias current is applied. As a trade-off between the achievable system bandwidth and the adverse effect of nonlinearity, the bias current is set to 120 mA and the corresponding –3dB bandwidth is about 32 MHz.

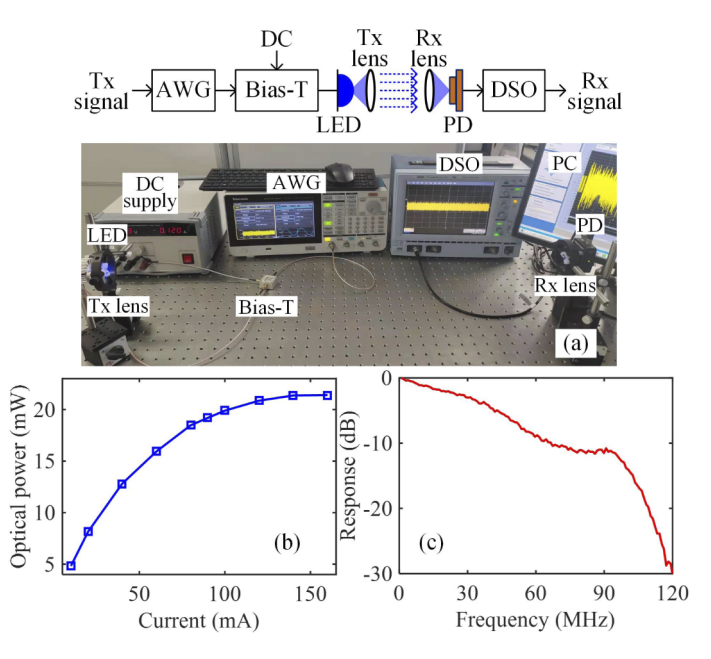


Fig. 5. Experimental setup of a point-to-point VLC system using a blue mini-LED. Insets: (a) the photo of the overall experimental system, (b) the measured nonlinear optical power-current curve and (c) the measured frequency response with a bias current of 120 mA

In our experiments, in accordance with the above simulations, we consider the following two cases: 1) N = 4 and k = 1; 2) N = 4 and k = 2. During the offline signal processing, the size of IFFT/FFT is 256, while the numbers of data subcarriers are 118 and 108 for k = 1 and 2, respectively. Given the AWG sampling rate of 250 MSa/s, the signal bandwidths for k = 1 and 2 are about 115 and 105 MHz, respectively. Hence, the corresponding transmission data rates for k = 1 and 2 are 172.5 and 210 Mbits/s, respectively.

Figure 6 shows the BER versus the peak-to-peak voltage (Vpp) of AWG output signals for two different cases, where the transmission distance is fixed at 90 cm. For N=4 and k=1, as shown in Fig. 6(a), the BER of DFT-S-OFDM-IM is slightly worse than that of OFDM-IM, which is due to the high PAPR of DFT-S-OFDM-IM as discussed in Section 3.1. It can be clearly seen that OFDM-QIM greatly outperforms both OFDM-IM and DFT-S-OFDM-IM, which achieves the lowest BER of 4.4×10^{-3} at Vpp = 2 V. Compared with OFDM-QIM, DFT-S-OFDM-QIM can achieve further significant BER improvement, which obtains the lowest BER of 1.0×10^{-3} at Vpp = 3 V. In contrast, as shown in Fig. 6(b), DFT-S-OFDM-IM performs much better than OFDM-IM when k is increased from 1 to 2. Moreover, OFDM-IM, DFT-S-OFDM-IM and OFDM-QIM achieve the lowest BER at the same Vpp of 2 V, while DFT-S-OFDM-QIM achieves the lowest BER 1.9×10^{-3} at Vpp = 3 V. For both cases, the optimal Vpp for DFT-S-OFDM-QIM is larger than that of other benchmark schemes, indicating its excellent tolerance against LED nonlinearity, which is mainly due to its superior PAPR performance. The corresponding constellation diagrams are depicted in insets (1)-(9) in Fig. 6.

Figure 7 shows the BER versus the transmission distance for different schemes, where the optimal Vpp is applied for each scheme. As we can see, the BER of every scheme is gradually

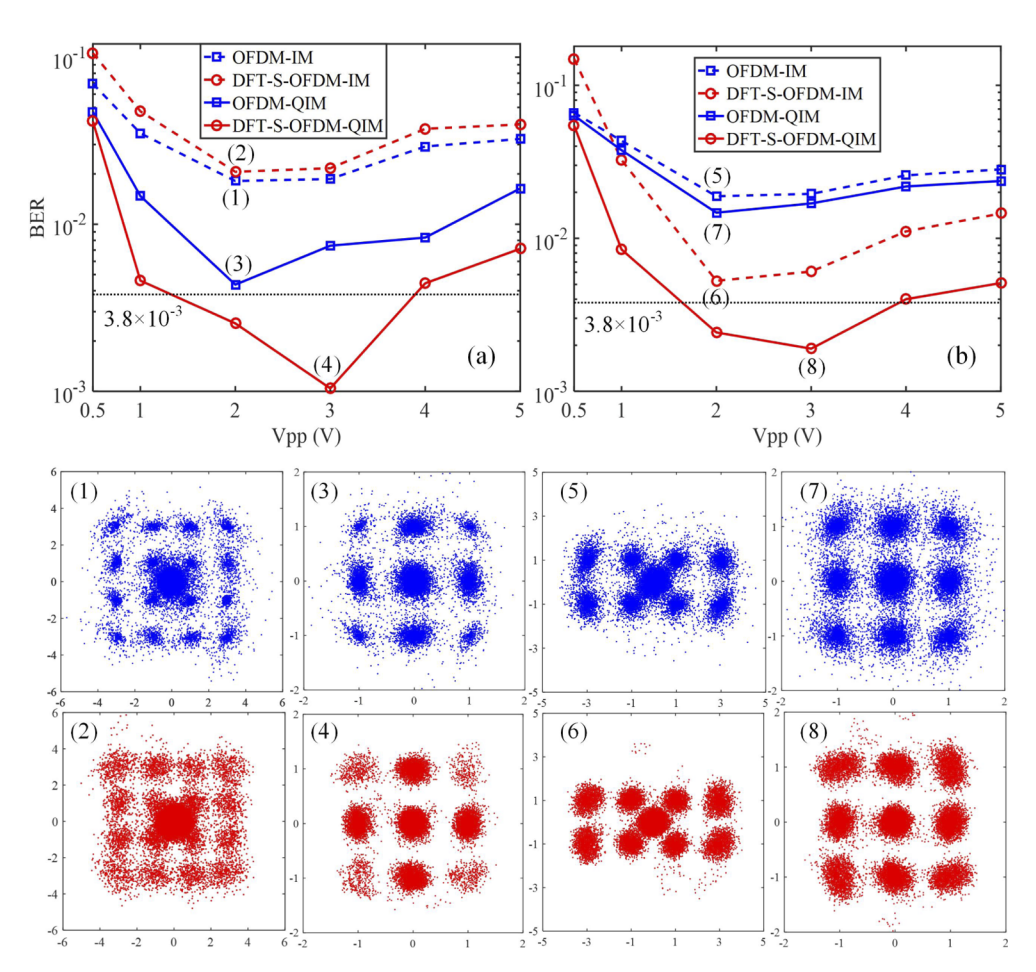


Fig. 6. BER vs. Vpp for OFDM-IM, DFT-S-OFDM-IM, OFDM-QIM and DFT-S-OFDM-QIM with (a) N = 4, k = 1 and (b) N = 4, k = 2 with a transmission distance of 90 cm. Insets (1)-(9) show the corresponding constellation diagrams.

increased with the extension of transmission distance for both k=1 and 2. Specifically, for N=4 and k=1 as shown in Fig. 7(a), the BERs of OFDM-IM and DFT-S-OFDM-IM cannot reach the FEC limit of 3.8×10^{-3} when the distance is in the range of 80 to 110 cm. Moreover, the maximum distances that can be transmitted by OFDM-QIM and DFT-S-OFDM-QIM below BER = 3.8×10^{-3} are 87.5 and 108.1 cm, respectively. As a result, a distance extension of 20.6 cm is obtained by DFT-S-OFDM-QIM in comparison to OFDM-QIM, which is corresponding to a 23.5% improvement of transmission distance. For N=4 and k=2, as shown in Fig. 7(b), OFDM-IM and OFDM-QIM cannot reach the FEC limit of BER = 3.8×10^{-3} for the distance within the range of 70 to 100 cm. In contrast, the maximum transmission distances achieved by DFT-S-OFDM-IM and DFT-S-OFDM-QIM are 84.1 and 97.5 cm, respectively. Hence, DFT-S-OFDM-QIM achieves a distance improvement of 15.9% compared with DFT-S-OFDM-IM.

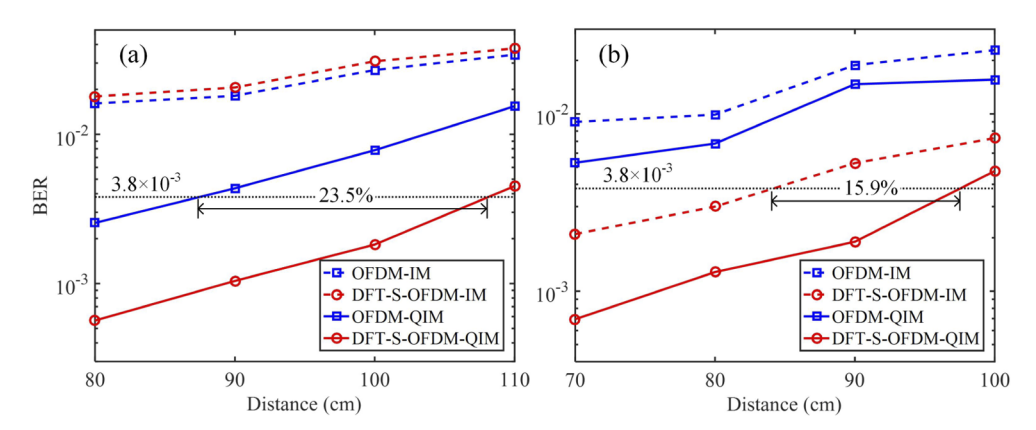


Fig. 7. BER vs. transmission distance for OFDM-IM, DFT-S-OFDM-IM, OFDM-QIM, and DFT-S-OFDM-QIM with (a) N = 4 and k = 1, (b) N = 4 and k = 2.

4. Conclusion

In this paper, we have proposed and evaluated a novel DFT-S-OFDM-QIM scheme for practical VLC systems with LED nonlinearity. Owing to the parallel index modulation on both the in-phase and quadrature components of each subcarrier, OFDM-QIM obtains a higher SE than conventional OFDM-IM. Moreover, DFT spreading has been shown to be a very efficient way to reduce the PAPR of OFDM-QIM, and DFT-S-OFDM-QIM exhibits much lower PAPR than OFDM-QIM and DFT-S-OFDM-IM for both cases of N=4 with k=1 and 2. Simulation results validate the excellent BER and PAPR performance of the proposed DFT-S-OFDM-QIM scheme over the AWGN channel. Furthermore, experimental results show that DFT-S-OFDM-QIM can use a larger Vpp to achieve the minimum BER than other benchmark schemes, which suggests that DFT-S-OFDM-QIM enjoys enhanced tolerance against LED nonlinearity. Specifically, a distance extension of 23.5% is obtained by DFT-S-OFDM-QIM compared with OFDM-QIM for the case N=4 and k=1, while a distance improvement of 15.9% is achieved by DFT-S-OFDM-IM in comparison to DFT-S-OFDM-IM for the case N=4 and k=2. Therefore, the proposed DFT-S-OFDM-QIM scheme reveals great potential for practical nonlinear VLC systems.

Funding. National Natural Science Foundation of China (61901065); Fundamental Research Funds for the Central Universities (2021CDJQY-013); China Postdoctoral Science Foundation (2021M693744).

Disclosures. The authors declare that there are no conflicts of interest related to this article.

Data availability. The data underlying the results presented in this paper are not publicly available at this time but may be obtained from the authors upon reasonable request.

References

- N. Chi, Y. Zhou, Y. Wei, and F. Hu, "Visible light communication in 6G: Advances, challenges, and prospects," IEEE Veh. Technol. Mag. 15(4), 93–102 (2020).
- I. Demirkol, D. Camps-Mur, J. Paradells, M. Combalia, W. Popoola, and H. Haas, "Powering the Internet of Things through light communication," IEEE Commun. Mag. 57(6), 107–113 (2019).
- C. Chen, S. Fu, X. Jian, M. Liu, X. Deng, and Z. Ding, "NOMA for energy-efficient LiFi-enabled bidirectional IoT communication," IEEE Trans. Commun. 69(3), 1693–1706 (2021).
- T. Komine and M. Nakagawa, "Fundamental analysis for visible-light communication system using LED lights," IEEE Trans. Consum. Electron. 50(1), 100–107 (2004).
- S. Rajagopal, R. D. Roberts, and S.-K. Lim, "IEEE 802.15.7 visible light communication: modulation schemes and dimming support," IEEE Commun. Mag. 50(3), 72–82 (2012).
- X. Deng, S. Mardanikorani, Y. Wu, K. Arulandu, B. Chen, A. M. Khalid, and J.-P. M. Linnartz, "Mitigating LED nonlinearity to enhance visible light communications," IEEE Trans. Commun. 66(11), 5593–5607 (2018).
- H. Le Minh, D. O'Brien, G. Faulkner, L. Zeng, K. Lee, D. Jung, and Y. Oh, "High-speed visible light communications using multiple-resonant equalization," IEEE Photonics Technol. Lett. 20(14), 1243–1245 (2008).

- 8. Y.-F. Liu, Y. C. Chang, C.-W. Chow, and C.-H. Yeh, "Equalization and pre-distorted schemes for increasing data rate in in-door visible light communication system," in *Opt. Fiber Commun. Conf.* (OFC, 2011), paper JWA83.
- C. Chen, Y. Nie, M. Liu, Y. Du, R. Liu, Z. Wei, H. Y. Fu, and B. Zhu, "Digital pre-equalization for OFDM-based VLC systems: Centralized or distributed?" IEEE Photonics Technol. Lett. 33(19), 1081–1084 (2021).
- H. Elgala, R. Mesleh, and H. Haas, "Indoor broadcasting via white LEDs and OFDM," IEEE Trans. Consum. Electron. 55(3), 1127–1134 (2009).
- 11. D. Tsonev, H. Chun, S. Rajbhandari, J. J. D. McKendry, S. Videv, E. Gu, M. Haji, S. Watson, A. E. Kelly, G. Faulkner, M. D. Dawson, H. Haas, and D. O'Brien, "A 3-Gb/s single-LED OFDM-based wireless VLC link using a Gallium Nitride µLED," IEEE Photonics Technol. Lett. 26(7), 637–640 (2014).
- C. Chen, X. Zhong, S. Fu, X. Jian, M. Liu, H. L. Yang, A. Alphones, and H. Y. Fu, "OFDM-based generalized optical MIMO," J. Lightw. Technol. (2021), early access.
- H. Marshoud, V. M. Kapinas, G. K. Karagiannidis, and S. Muhaidat, "Non-orthogonal multiple access for visible light communications," IEEE Photonics Technol. Lett. 28(1), 51–54 (2016).
- B. Lin, W. Ye, X. Tang, and Z. Ghassemlooy, "Experimental demonstration of bidirectional NOMA-OFDMA visible light communications," Opt. Express 25(4), 4348–4355 (2017).
- C. Chen, W.-D. Zhong, H. Yang, and P. Du, "On the performance of MIMO-NOMA based visible light communication systems," IEEE Photonics Technol. Lett. 30(4), 307–310 (2018).
- B. Lin, Q. Lai, Z. Ghassemlooy, and X. Tang, "A machine learning based signal demodulator in NOMA-VLC," J. Lightwave Technol. 39(10), 3081–3087 (2021).
- K. Ying, Z. Yu, R. J. Baxley, H. Qian, G.-K. Chang, and G. T. Zhou, "Nonlinear distortion mitigation in visible light communications," IEEE Wireless Commun. 22(2), 36–45 (2015).
- J. Li, Z. Huang, X. Liu, and Y. Ji, "Hybrid time-frequency domain equalization for LED nonlinearity mitigation in OFDM-based VLC systems," Opt. Express 23(1), 611–619 (2015).
- Y. Wang, L. Tao, X. Huang, J. Shi, and N. Chi, "Enhanced performance of a high-speed WDM CAP64 VLC system employing Volterra series-based nonlinear equalizer," IEEE Photonics J. 7(3), 1–7 (2015).
- 20. E. Başar, "Index modulation techniques for 5G wireless networks," IEEE Commun. Mag. 54(7), 168–175 (2016).
- E. Başar, Ü. Aygölü, E. Panayırcı, and H. V. Poor, "Orthogonal frequency division multiplexing with index modulation," IEEE Trans. Signal Process 61(22), 5536–5549 (2013).
- 22. E. Başar and E. Panayırcı, "Optical OFDM with index modulation for visible light communications," in *Int. Workshop Opt. Wireless Commun.* (IWOW, 2015), 11–15.
- C. Chen, X. Deng, Y. Yang, P. Du, H. Yang, and W. Zhong, "Experimental demonstration of optical OFDM with subcarrier index modulation for IM/DD VLC," in *Conference on Asia Communications and Photonics* (ACP, 2019), paper M4A.40.
- M. Wen, B. Ye, E. Başar, Q. Li, and F. Ji, "Enhanced orthogonal frequency division multiplexing with index modulation," IEEE Trans. Wireless Commun. 16(7), 4786–4801 (2017).
- C. Chen, W.-D. Zhong, H. Yang, S. Zhang, and P. Du, "Reduction of SINR fluctuation in indoor multi-cell VLC systems using optimized angle diversity receiver," J. Lightwave Technol. 36(17), 3603–3610 (2018).